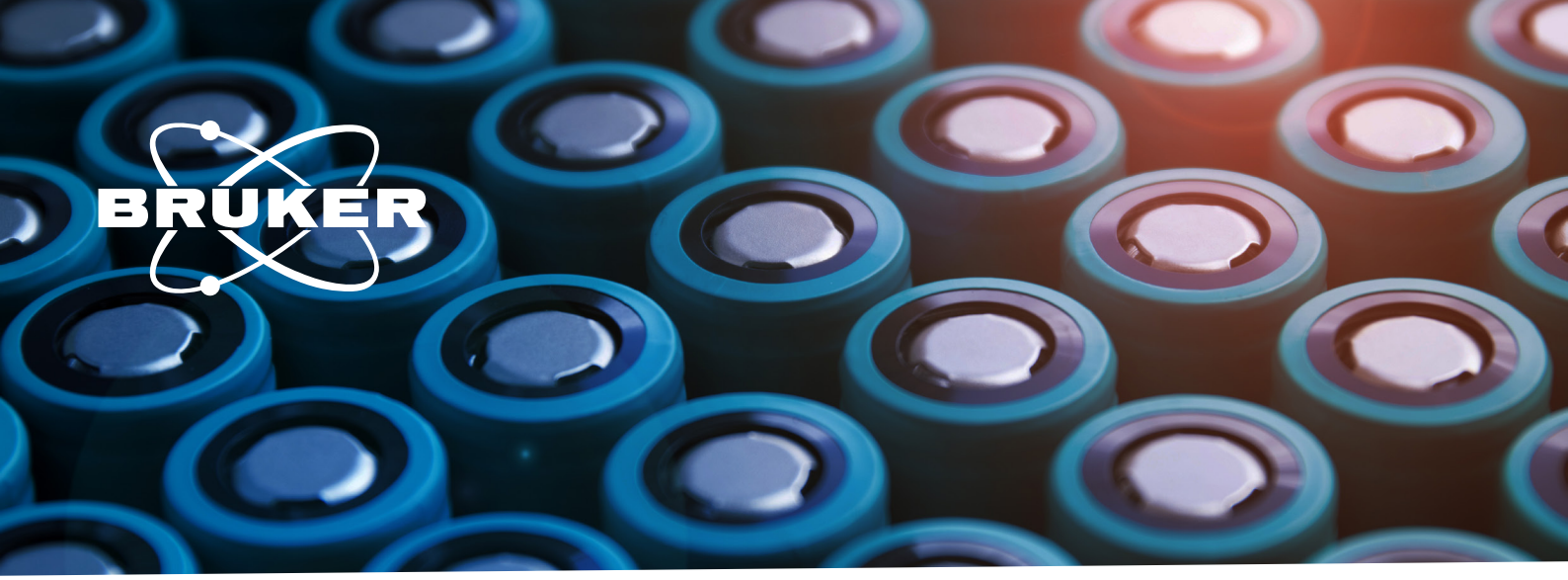

# EPR

# *In-Situ* EPR Imaging Sheds Light on Size and Distribution of Metallic Deposits in Lithium-Ion Batteries

Innovation with Integrity

Lithium-ion batteries (LIB) are vital to power new electric vehicles and rechargeable portable electronic devices. As demand for ever greater performance continues to surge, researchers must address some of the limitations that persist in LIB design, such as the build-up of Lithium (Li) deposits around the anode during charging. Precise and sensitive *in-situ* analytical methods are needed to better understand the underlying chemistry of LIB materials and overcome such limitations. Electron paramagnetic resonance (EPR) spectroscopy is one of several magnetic resonance technologies that enables researchers to measure metallic Lithium (Li) deposits non-invasively, emulating real life conditions. This app note describes the use of EPR imaging (EPRI) to evaluate the distribution of Li deposits and their microstructural characteristics.

## Introduction

The growing concerns around climate change prompting the need for alternative energy solutions to reduce greenhouse gas emissions is driving research efforts to optimize battery materials, improve transport properties of target ions, and lower costs. In addition to portable devices such as laptops and smartphones, rechargeable batteries are increasingly commonplace in transport, due to the growing popularity of electric cars. Lithium-ion batteries (LIB) are currently one of the most popular options, owing to lithium's high energy density and electrochemical potential, and are widely used across the globe.

An important feature of LIBs is the solid-electrolyte interphase (SEI) – a layer that builds up during the battery's first charging cycle and prevents the anode material from decomposing. However, LIBs and other rechargeable batteries are limited by the phenomenon of dendrite growth – the accumulation of metallic Li deposits in a process known as 'plating'. While most plated Li can be reversibly 'stripped', where it undergoes charge transfer into the electrolyte and can be re-intercalated into the anode, some part will be consumed irreversibly due to the reaction with the electrolyte, forming new SEI film.[1] Another small part can form 'dead Li', which is electrically isolated from the anode and contributes to the degradation of a LIB's lifespan. Li dendrites can build up over the battery's lifetime, not only impacting its performance, but potentially causing it to short-circuit if the dendrite pierces the electrical separator.

An understanding of the microstructural characteristics of dendrites, growth mechanisms, and the plating/stripping process is crucial to progressing LIB research and ensuring the safety of batteries.
Advanced *in-situ* measurement techniques are required to achieve this and to develop the next generation of LIBs. Developments in magnetic resonance spectroscopy, including nuclear magnetic resonance (NMR) and electron paramagnetic resonance (EPR) spectroscopy, and imaging techniques such as magnetic resonance imaging (MRI), are paving the way for this progress.

In this study, researchers from the Shanghai Key Laboratory of Magnetic Resonance, East China Normal University, China, recorded the semiquantitative distribution of Li deposits on the electrode plane at different plating and stripping stages via *in-situ* spatial–spatial EPR imaging (EPRI).[2] Spectral—spatial EPRI was also carried out, to estimate the Li microstructural dimensions at different deposition sites and operando EPR spectra were obtained to characterize plating/stripping behaviour.

## Materials & methods

An anode-free battery system was used to study the deposition behavior of Li metal, to minimize the influence of the Li substrate on the EPR spectra. The cathode was composed of $LiCoO_2$ (LCO) powder (Alfa, 99.5 %), Ketienblack, and poly(vinylidene difluoride) (PVDF) in a weight ratio of 90:2.5:7.5. In the EPR cell, the Coulombic efficiency (CE) of the cathode should be higher than that of the anode to ensure the complete stripping of Li deposits. LCO has a high initial CE when cycling below 4.25 V.

An aluminum foil was used as the current collector. The anode was composed of bare copper (Cu) foil to plate Li metal, with the remaining surface covered with Kapton tapes. The cathode, the separator, and the anode were wrapped with Kapton tapes and soaked in electrolyte (1 M $LiPF_6$ in a mixture of ethylene carbonate (EC), dimethyl carbonate (DMC), and ethyl methyl carbonate (EMC) with 5 % additive of fluoroethylene carbonate (FEC)).

## Operando EPR

Continuous-wave (CW) EPR spectra were recorded at X-band on a Bruker ELEXSYS E580 spectrometer equipped with a Super High Sensitivity cavity (SHQE-W1) for five charge/discharge cycles. EPR spectra were recorded in real time during charge and discharge to monitor the evolution of the Li signal. The electrode plane was placed parallel to the main magnetic field. The first two charges were divided into three segments and the first two discharges were divided into two segments. At the end of each segment, the cell was held in an open circuit for 30 min before conducting *in-situ* EPRI.

## *In-situ* EPRI

The two-dimensional (2D) spatial—spatial and spectral—spatial EPRI measurements were carried out with a field of view of 10 mm. To generate the spatial—spatial images, reference spectra were recorded without gradient field and the projection spectra were deconvoluted from these reference spectra. The results were filtered and back-projected to obtain the final images. For spectral—spatial imaging, the projection spectra were directly filtered and back-projected to generate the final images.

## Results & discussion

In EPR spectra of Li metal, it is known that lineshape is associated with Li microstructures and that the ratio of diffusion time ($T_D$) to the spin—spin relaxation time ($T_2$) is the main parameter contributing to the lineshape. The spectrum of conduction EPR can be loosely represented by the spectral intensity, the linewidth (ΔB) and the asymmetry ratio (A/B), as illustrated in Figure 1.

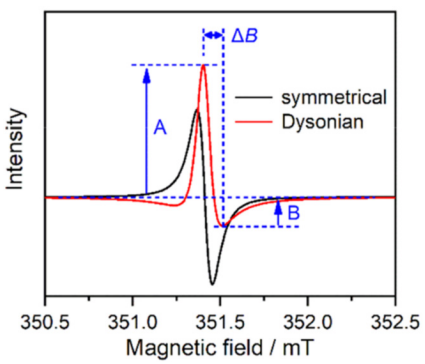


**Figure 1:** Schematic for the symmetrical lineshape and the Dysonian lineshape. ΔB denotes the line width from peak to peak. A and B denote the distance between the positive/negative peak and the baseline, respectively. Reproduced from reference 2 in accordance with Creative Commons Attribution License 4.0.

## Operando EPR

The signal intensity was found to grow linearly during the first 15 min of the first charge, where the Li metal began to nucleate on the Cu foil. The linewidth was about 0.2 mT at the beginning of plating and during the first open circuit volume (OCV) period, ΔB increased slightly, which could be related to the Li surface reaction. After further plating, ΔB decreased and was maintained at around 0.1 mT. The variation in ΔB is thought to be due to the surface relaxation. The A/B correlates to the size of the Li microstructures in the deposits and during plating, an almost linear increase in A/B was observed which indicates the thickening of the Li deposits.
The total time of the first discharge was 239.9 min (Figure 2a1,a2), delivering an initial CE of 94.1 %, which was below the initial CE of the LCO used. The CE is therefore determined by the plating/stripping efficiency. The irreversible Li losses can be attributed to the SEI formation with a side reaction and dead Li (the disconnection of the Li microstructures from the conductive network). For the electrolyte containing an FEC additive, the capacity loss due to the SEI Li accounts for the major irreversible Li capacity.

The g factor – a scaling factor to account for coupling between the electrons' orbital spin and angular momentum – of the Li signal remained unchanged (Figure 2b1,b2) and the peak-to-peak intensity decreased (Figure 2c1,c2) upon stripping. Interestingly, the intensity did not attenuate during the OCV periods in the discharge process, which indicates that the microscopic process of stripping is different. Upon plating, the newly deposited Li would pierce the SEI, becoming exposed to the electrolyte, while the SEI always covers the Li surface upon stripping, suppressing the side reaction.

The linewidth ΔB increased from around 0.1 to 0.38 mT during the first discharge (Figure 2d1, d2) due to the thinner deposits with a stronger surface-relaxation effect. During the last 30 min of discharge, ΔB declined rapidly to 0.1 mT. The residual signal is attributed to the dead Li, confirming that the reversibility is subject to the anode. Although an abrupt change in lineshape is observed, it is difficult to determine when some parts of Li deposits lose electrical contact as the signal of the dead Li is 'buried' in the signal of Li deposits and emerge as the electrically active Li is stripped.

## *In-situ* spatial—spatial EPRI

The thickness of Li deposits, or deposit quantity, was calculated using spatial—spatial EPRI to determine the nucleation sites. Figure 3a shows that the profile of the Li deposits was consistent with the plating area, and that metallic Li primarily nucleates on the corners of the Cu foil. The cell states at the end of each segment are denoted as 1Ci, 1Cii, and 1Ciii for the first charge, 1Di and 1Dii for the first discharge, and so on.

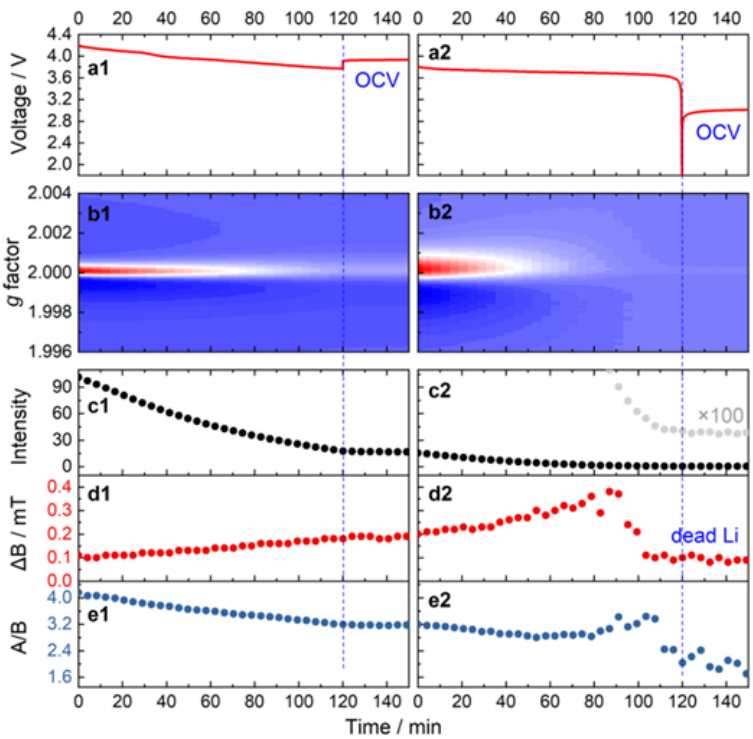


**Figure 2:** Operando electron paramagnetic resonance (EPR) results for the first discharge. The discharge process is divided into two segments to perform EPR imaging (EPRI) after each segment. **(a1, a2)** Voltage profiles of the LCO || Cu cell. **(b1, b2)** Projected operando EPR spectra, in which the maximum, the median, and the minimum are mapped to red, white, and blue, respectively. Evolution of **(c1, c2)** the peak-to-peak intensity, **(d1, d2)** the linewidth ΔB, and **(e1, e2)** the asymmetry ratio A/B as a function of time. The vertical dashed line indicates the beginning of the open-circuit voltage (OCV) period. Reproduced from reference 2 in accordance with Creative Commons Attribution License 4.0.

The pixel resolution of EPRI is proportional to the linewidth ΔB and inversely proportional to the gradient strength. Four distinct sites indicate local excessive deposits (LEDs), which could be attributed to the growth of dendritic Li (Figure 3b), and the number of sites increased between 1Cii and 1Ciii (Figure 3c). During the first discharge, Li stripping can be observed (Figure 3d), with most LEDs fading after the first stripping. The distribution of dead Li can be seen clearly in Figure 3e and, when compared with Figure 3d, dead Li is strongly correlated with LEDs.

At the beginning of the second charge, the metallic Li nucleates on the Cu foil again. The second deposition concentrated on the sites of the previous LEDs, around the margin of the Cu foil and, surprisingly, the sites for dead Li were preferred for secondary deposition. Plating then continued to take place on the sites of LEDs. The thickness and positions of the LEDs for 2Cii were similar to those of 1Ciii, although fewer in quantity. In addition, metallic Li was plated homogenously during the first plating, before LED growth, but during the second plating, LEDs appeared before homogenous plating.

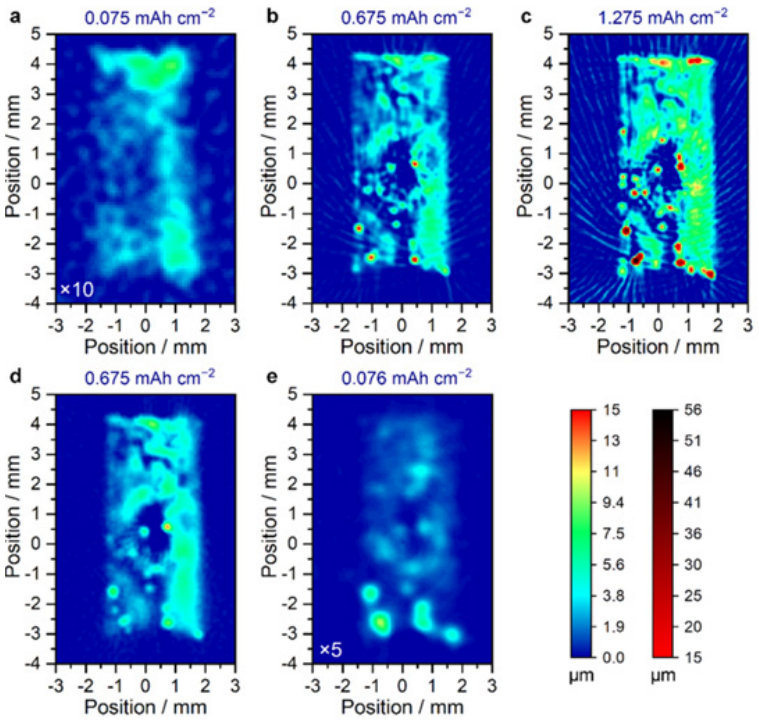


**Figure 3:** *In-situ* spatial–spatial electron paramagnetic resonance imaging (EPRI) for the first cycle. **(a–c)** Images of the pouch cell at the end of three charge periods (1Ci, 1Cii, and 1Ciii). **(d, e)** Images of the pouch cell at the end of two discharge periods (1Di and 1Dii). All images share one set of a color bar with the pseudothickness values. The signal intensities in **(a)** and **(e)** are multiplied by 10 and 5, respectively, for better contrast. The theoretical quantity of Li deposits without regard to the side reaction is labeled on the top of each image. The pixel sizes of **(a–e)** are 200, 100, 100, 100, and 100 μm, respectively. A slight drift of the gradient center after 1Cii is due to the restart of the equipment. Reproduced from reference 2 in accordance with Creative Commons Attribution License 4.0.

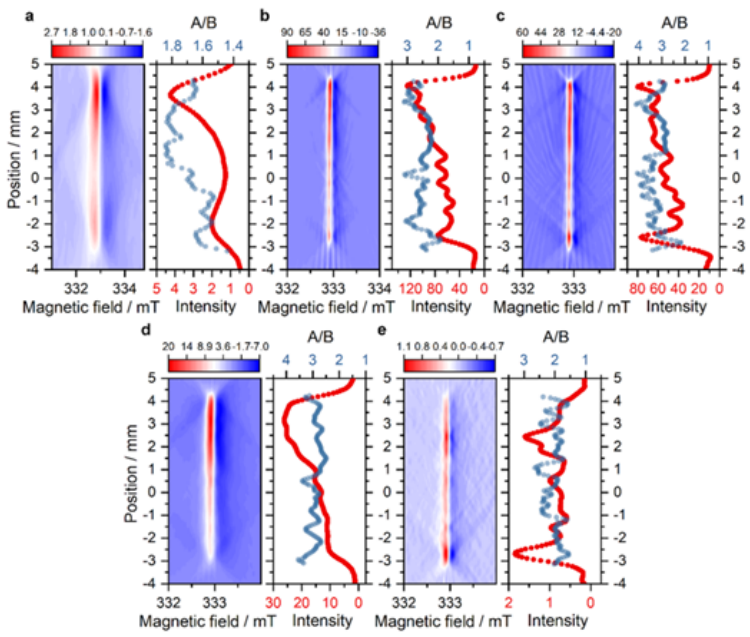


**Figure 4:** *In-situ* spectral–spatial electron paramagnetic resonance imaging (EPRI) for the first cycle. **(a–e)** Spectral–spatial images (left) and the plots of the intensity and the A/B values (right) along the Y-axis for 1Ci, 1Cii, 1Ciii, 1Di, and 1Dii, respectively. The spatial resolutions of **(a–e)** are 200, 100, 100, 100, and 100 μm, respectively. Reproduced from reference 2 in accordance with Creative Commons Attribution License 4.0.

## *In-situ* spectral—spatial EPRI

Figure 4a shows the A/B for 1Ci, indicating that the size of Li varies slightly at nucleation. Since A/B increased with deposit thickness, Li metal was shown not to deposit compactly on the Cu foil from the start of plating. Four LEDs were observed in the 1Cii EPRI image (Figure 4b) and for 1Ciii, more LEDs are seen to be scattered (Figure 4c). Some peaks in the A/B plot have strong relevance to the number of LEDs, indicating that some may also be composed of compact deposits.

The intensity plot becomes smooth for 1Di, but with fluctuations in the A/B plot (Figure 4d). At the end of the first discharge, the sizes of the dead Li are not uniform, as A/B oscillates (Figure 4e).

The fluctuations in the A/B plots intensified during the second plating, with Li plating for 2Ciii mainly occurring in the homogenous areas. Although the thickness of the Li deposits was unevenly distributed, the sizes of the Li microstructures seemed to become homogenous upon stripping.

## Conclusion

This study demonstrates a strategy, using an anode-free LIB, to investigate the plating and stripping behavior of metallic Li using *in-situ* EPRI. These methods allow both, academic and industrial researchers to test LIBs under conditions closely representing a practical battery system, thanks to the non-invasive EPR technology. 2D spatial—spatial imaging provides semiquantitative information on the Li deposit distribution, and here it revealed that some LEDs were formed during plating, primarily during the second plating, which was a major cause of dead Li during stripping.

Spectral—spatial EPRI showed that LEDs were composed of both dendritic-size Li and thick Li metals, and that the homogeneity of the Li microstructures became poorer after cycling. These findings will provide researchers with a deeper understanding of the evolution of Li microstructures during repeated plating and stripping, and therefore contribute to improving LIB design and efficiency.

Bruker's solution portfolio for battery research, product innovation and quality control incorporate EPR and NMR instruments ranging from easy-to-use benchtop devices to highly sophisticated floor-standing systems. This offering ensures the broadest value-chain coverage from early-stage innovation to final products including harmonized methods and maximized result comparability.

## About Bruker Corporation

Bruker is enabling scientists to make breakthrough discoveries and develop new applications that improve the quality of human life. Bruker's high-performance scientific instruments and high-value analytical and diagnostic solutions enable scientists to explore life and materials at molecular, cellular and microscopic levels. In close cooperation with our customers, Bruker is enabling innovation, improved productivity and customer success in life science molecular research, in applied and pharma applications, in microscopy and nanoanalysis, and in industrial applications, as well as in cell biology, preclinical imaging, clinical phenomics and proteomics research and clinical microbiology. For more information, please visit www.bruker.com

## References:


1. Ren, D., Smith, K., Guo, D., et al. Investigation of Lithium Plating-Stripping Process in Li-Ion Batteries at Low Temperature Using an Electrochemical Model, J Electrochem Soc, 165, A2167 (2018).
2. Geng, F., Yang, Q., Li, C., et al. Mapping the Distribution and the Microstructural Dimensions of Metallic Lithium Deposits in an Anode-Free Battery by *In-situ* EPR Imaging, Chem Mater, 33(21), 8223-8234 (2021).



Bruker BioSpin is continually improving its products and reserves the right to change specifications without notice. Order No. T188289 © 02/2024 Bruker BioSpin.



**Bruker BioSpin**
info@bruker.com

bruker.com


**Customer Support**
https://www.bruker.com/en/services/support.html

**Online information**
bruker.com/